NASA Technical Memorandum 82768

NASA-TM-82768 19820011797

NASA TM-82768

Mechanism and Models for Zinc Metal Morphology in Alkaline Media

Charles E. May and Harold E. Kautz
Lewis Research Center
Cleveland, Ohio

December 1981

NASA

MECHANISM AND MODELS FOR ZINC METAL MORPHOLOGY IN ALKALINE MEDIA

by Charles E. May and Harold E. Kautz

National Aeronautics and Space Administration
Lewis Research Center
Cleveland, Ohio

SUMMARY

Based on experimental observations, a mechanism is presented to explain the existence of the different morphologies of electrodeposited zinc in alkaline solution. The high current density dendrites appear to be due to more rapid growth on the non-basal crystallographic planes than on the basal plane. The low current density moss apparently results from dissolution from the non-basal planes at low cathodic voltages.

Electrochemical models were sought which would produce such a phenomenon. The fundamental plating mechanism alone can account only for different rates on different planes, not for zinc dissolution from a plane in the cathodic region. Fourteen models were explored; two models were found to be in accord with the proposed mechanism. One involves rapid disproportionation of the zinc +1 species on the non-basal planes. The other involves a redox reaction (corrosion) between the zinc-zincate and hydrogen-water systems.

INTRODUCTION

An important aspect of the alkaline zinc electrode is the morphology of the zinc which is electrodeposited during charging (refs. 1 and 2). At low current density and high zincate concentration, the morphology of the zinc is termed mossy. This zinc is in the form of fine whiskers reported to be of micrometer diameter (ref. 3). At higher current densities and low zincate concentrations, boulders (nodules) of zinc form (ref. 4). These are macrocrystalline. At extremely low average current densities, a smooth plate of zinc is attainable (ref. 5) and at extremely high current densities, dendritic zinc is formed. The morphology is also affected by the presence of impurities (ref. 6).

Because the boulder and dendritic morphologies lead to shorting, the mossy form is generally preferred for battery applications (ref. 7). It would be very useful to preserve the mossy form at higher current densities in order to increase the rate of charging without favoring shorting. A knowledge of the mechanism of the mossy morphology would be highly desireable. Generally, the morphology is examined from the viewpoint of why dendrites grow (refs. 5 and 8).

The purpose of this report is to present and discuss a possible mechanism for the formation of the various zinc morphologies and propose several models that can give rise to this mechanism. Emphasis is placed on an explanation of the mossy deposit. Many of the concepts presented here should be applicable to the plating of other metals.

According to our proposed mechanism, the mossy zinc morphology is due to the dissolution of zinc from the non-basal crystallographic planes at low cathodic voltages. Two models were found to be in accord with this mechanism. One involves rapid disproportionation of the zinc +1 species on the

E-1090

non-basal planes. The other involves a redox reaction between the zinc-zincate and hydrogen-water systems.

OBSERVATIONS LEADING TO THE MECHANISM

Figure 1 is a Scanning Electron Microscope (SEM) view of dendritic zinc deposited at high voltage and high current density. Note that the dendrites are composed of shingled hexagonal plates. It seems clear that the faces of these plates are the basal planes of the hexagonal zinc crystal lattice. The edges of these plates are non-basal planes. One concludes that in the dendritic deposition region, zinc plates much more rapidly on the non-basal $1\bar{1}00$, $10\bar{1}0$, and $01\bar{1}0$ planes than on the basal faces for thin plates to form. In this report, reference to non-basal planes and N planes indicate the $1\bar{1}00$, $10\bar{1}0$, and $01\bar{1}0$ planes; reference to the B plane refers to the basal plane.

Figure 2(a) is an SEM view of mossy zinc deposited at low voltage and low current density. Unlike the dominating two dimensional growth of dendrites, the moss grows predominantly in one dimension. The lack of facets or other crystal-like appearance suggests that the zinc may not be crystalline. We have, however, obtained X-ray and electron diffraction patterns that show the moss strands to be the hexagonal zinc crystal structure. Figures 2(b) and (c) are respectively a Transmission Electron Microscope (TEM) view of a mossy zinc strand and an electron diffraction pattern taken on that strand. The pattern in figure 2(c) proves that the strand shown in figure 2(b) is single crystal zinc and that the cross section of the strand coincides with the basal plane. This orientation indicates that for a mossy deposit, zinc plates much more rapidly on the basal plane than on the non-basal sides of the strands. Therefore, it appears at first that the relative rates of plating on the basal and non-basal planes determine which morphology (dendrites or moss) will form.

However, two observations concerning the moss seem somewhat contradictory. They are: (1) the strands of moss are single crystals and (2) the SEM pictures never display any typical crystal growth facets. A way to resolve this apparent contradiction is to assume that zinc is, in fact, dissolving off the non-basal planes during the deposition of the mossy zinc: dissolving crystals tend to lose their faceting and become more rounded.

Figure 3 is an SEM picture of zinc crystal growth at conditions intermediate between the high voltage (non-basal dominating) dendrites, and the low voltage (basal dominating) moss. These "boulders" display typical hexagonal crystal shape with comparable plating rates on basal and non-basal planes.

To explain these observations, our proposed mechanism is the following. At low cathodic overvoltages, zinc plates on the basal plane but dissolves off the non-basal plane, giving rise to the whiskers called moss. At intermediate voltages, zinc begins to plate on both sets of planes. The rates on both sets of planes are comparable so that boulders result. At high voltages, the rate of deposit on the non-basal planes exceed that of the basal plane. The dendrites result.
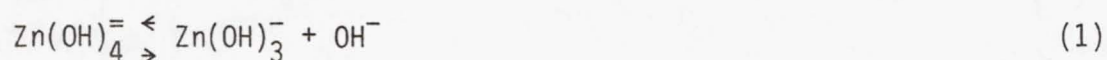
THEORETICAL MODELS

The next step is to examine models to find one or more which can give rise to the proposed mechanism. The models consist of the electrochemical and chemical reactions which are (or may be) involved as well as the applicable Butler-Volmer equations; in general two sets are required, one for the basal

and one for the non-basal planes. The chief test for a model is its ability to predict dissolution of zinc from the non-basal plane at low cathodic voltages.

Fourteen models (A to N) are examined. All of these assume steady state conditions, no concentration gradients between the bulk and plating surfaces, and a constant ratio between the B and N plane areas. Model A consists of the use of only the fundamental equations involved with the deposition of zinc and diffusion of species between the N and B planes. Each of the other models presented here use the equations operative in model A plus one additional proposed chemical (or electrochemical) reaction.

Model A

The equations involved in this model can be obtained from the work of Bockris et al. (ref. 9). They investigated the electrochemical mechanism for deposition of zinc from alkaline solution. Four reactions were found to be involved.

$$Zn(OH)_4^= \underset{\rightarrow}{\overset{\leftarrow}{}} Zn(OH)_3^- + OH^- \tag{1}$$

$$\overset{RDS}{Zn(OH)_3^- + e^- \underset{\leftarrow}{\overset{\rightarrow}{}} Zn(OH)_2^- + OH^-} \tag{2}$$

$$Zn(OH)_2^- \underset{\rightarrow}{\overset{\leftarrow}{}} ZnOH + OH^- \tag{3}$$

$$ZnOH + e^- \underset{\rightarrow}{\overset{\leftarrow}{}} Zn^0 + OH^- \tag{4}$$

Reaction (2) is the Rate Determining Step (RDS). Because reactions (1) and (3) are nonelectrochemical and in equilibrium, the mechanism may be abbreviated for our purposes. Reactions (1) and (2) may be combined into reaction (1-2) and reactions (3) and (4) may be combined into reaction (3-4).

$$\overset{RDS}{Zn(OH)_4^= + e^- \underset{\leftarrow}{\overset{\rightarrow}{}} Zn(OH)_2^- + 2\ OH^-} \tag{1-2}$$

$$Zn(OH)_2^- + e^- \underset{\rightarrow}{\overset{\leftarrow}{}} Zn^0 + 2\ OH^- \tag{3-4}$$

Looking at the reactions on the basal and non-basal planes individually allows one to generate four Butler-Volmer type equations. Such equations now involve the area fraction of basal and non-basal planes. To simplify the notation and manipulation of these equations, we express them as follows:

3

$$N_1 = N_2 \ (1 - X_N \ V^2)/V^{NA} \tag{5}$$

$$N_3 = N_4 \ (X_N - V^2)/V^{NB} \tag{6}$$

$$B_1 = B_2 \ (1 - X_B \ V^2)/V^{BA} \tag{7}$$

$$B_3 = B_4 \ (X_B - V^2)/V^{BB} \tag{8}$$

The N_1, N_3, B_1, and B_3 are currents per unit area; the N's refer to the non-basal planes while the B's refer to the basal plane; the subscript 1 refers to reactions (1-2) and the subscript 3 refers to reactions (3-4). The N_2, N_4, B_2, and B_4 are the products of the corresponding exchange current and the area fraction of the plane involved. (One should note that the areas include only those in the plating region and not regions which do not "feel" the plating overvoltage.) Because equation (1-2) is the rate determining step, either $B_2 \gg B_4$ or $N_2 \gg N_4$. The symbol V is equal to exp $(\bar{F}v/2RT)$ where v is the overvoltage and F is the Faraday. The NA, NB, BA, and BB are twice the corresponding symmetry factors. The X_N and X_B are the ratios of the concentration of the intermediate species $Zn(OH)_2^-$ at an overvoltage v compared with its concentration at $v = 0$. The concentration of the other species at the surface such as $Zn(OH)_4^=$ do not appear explicitly in equations (5) to (8) but are implicitly incorporated into the exchange currents. The surface concentrations of such species are assumed to be constant, independent of voltage. This is an oversimplification because concentration polarization does occur. But this simplification does not invalidate the results of this paper.

The concentration of the intermediate species $Zn(OH)_2^-$ on one plane is dependent on its value on the other plane because of possible diffusion from the plane with the higher concentration to the plane with the lower concentration.

$$Zn(OH)_2^- \text{ (one plane)} \rightarrow Zn(OH)_2^- \text{ (other plane)} \tag{9}$$
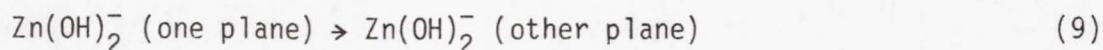
Mathematically the diffusion rate D_1 can be expressed as

$$D_1 = D_2 \ (X_N - X_B) \tag{10}$$

where D_2 is the rate constant which is dependent on the areas of each individual plane. If the facets of the individual planes are small, D_2 will be relatively large, allowing rapid diffusion. Again, for simplicity we consider D_2 to be constant for any one particular deposit. Equation (10) is written as if diffusion proceeded from the N planes to the B planes. If $X_B > X_N$ and the opposite occurs, D_1 will be negative. D_2 must be positive. The mathematical details of the model A are given in appendix A.

The results of our calculations are summarized in figures 4 to 7. In these figures R (N_3/N_5: plating on non-basal plane divided by plating on basal plane) is plotted against the cathodic overvoltages. Each figure (4 to 7) represents a different set of basic constants N_2, N_4, B_2, and B_4 while each subfigure (b) to (j) shows the effect of varying one of the nine rate constants. The plots show that the value of R can vary considerably with

voltage if an exponential constant of the rate controlling step is varied (See figs. 4(d), 4(i), 5(d), and 5(i)). The value of R can even be varied from above unity to below unity as a function of voltage if $N_2 > B_4 > N_4 > B_2$ (See fig. 7). This indicates that at low voltage, plating on the basal plane can dominate while at high voltages, plating on the non-basal planes can dominate. Moreover, in some cases R can even reach a maximum. Finally and most importantly, R cannot have a negative value in model A as implied in figures 4 to 7, and as shown algebraicly in appendix A. Model A alone would be acceptable if the mechanism did not require dissolution from the N planes at low cathodic voltages.

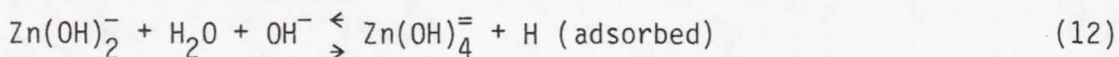## Other Models

Other possible models are easily devised by incorporating an auxiliary reaction into model A for each. Such reactions may involve disproportionation, simple corrosion, electrochemical corrosion, or catalytic redox. Some of these reactions are very likely to occur such as those involving electrochemical corrosion (ref. 10); some are not too likely. The 13 we tried are listed below. The equation given for a particular model is generally more discriptive than the model's name.
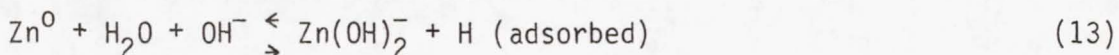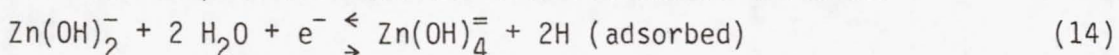
Model B Disproportionation

$$2Zn(OH)_2^- \underset{\rightarrow}{\overset{\leftarrow}{}} Zn^0 + Zn(OH)_4^= \tag{11}$$

Model C Nonelectrochemical oxidation

$$Zn(OH)_2^- + H_2O + OH^- \underset{\rightarrow}{\overset{\leftarrow}{}} Zn(OH)_4^= + H \text{ (adsorbed)} \tag{12}$$

Model D Nonelectrochemical corrosion

$$Zn^0 + H_2O + OH^- \underset{\rightarrow}{\overset{\leftarrow}{}} Zn(OH)_2^- + H \text{ (adsorbed)} \tag{13}$$

Model E Coupled chemical and electrochemical oxidation

$$Zn(OH)_2^- + 2 H_2O + e^- \underset{\rightarrow}{\overset{\leftarrow}{}} Zn(OH)_4^= + 2H \text{ (adsorbed)} \tag{14}$$
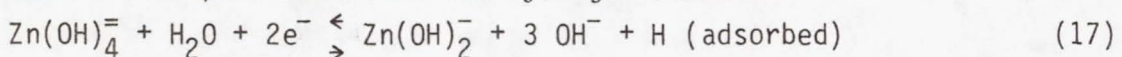
Model F Coupled chemical and electrochemical corrosion

$$Zn^0 + 2 H_2O + e^- \underset{\rightarrow}{\overset{\leftarrow}{}} Zn(OH)_2^- + 2H \text{ (adsorbed)} \tag{15}$$
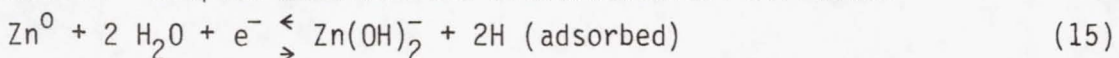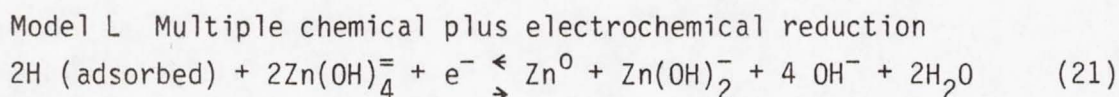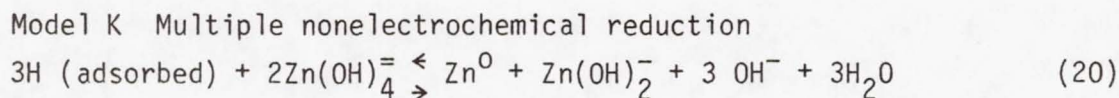
Model G Coupled plating and hydrogen formation

$$Zn(OH)_2^- + H_2O + 2e^- \underset{\rightarrow}{\overset{\leftarrow}{}} Zn^0 + 3 OH^- + H \text{ (adsorbed)} \tag{16}$$
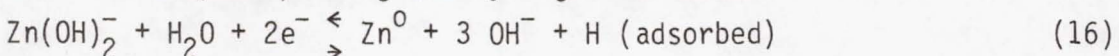
Model H Coupled reduction and hydrogen formation

$$Zn(OH)_4^= + H_2O + 2e^- \underset{\rightarrow}{\overset{\leftarrow}{}} Zn(OH)_2^- + 3 OH^- + H \text{ (adsorbed)} \tag{17}$$

Model I Catalytic plating

$$2Zn(OH)_2^- + e^- \rightleftharpoons Zn(OH)_2^- + Zn^0 + 2\ OH^- \qquad (18)$$

Model J Catalytic reduction

$$Zn(OH)_4^= + Zn(OH)_2^- + e^- \rightleftharpoons 2Zn(OH)_2^- + 2\ OH^- \qquad (19)$$

Model K Multiple nonelectrochemical reduction

$$3H\ (adsorbed) + 2Zn(OH)_4^= \rightleftharpoons Zn^0 + Zn(OH)_2^- + 3\ OH^- + 3H_2O \qquad (20)$$

Model L Multiple chemical plus electrochemical reduction

$$2H\ (adsorbed) + 2Zn(OH)_4^= + e^- \rightleftharpoons Zn^0 + Zn(OH)_2^- + 4\ OH^- + 2H_2O \qquad (21)$$

Model M Multiple electrochemical plus chemical reduction

$$H\ (adsorbed) + 2Zn(OH)_4^= + 2e^- \rightleftharpoons Zn^0 + Zn(OH)_2^- + 5\ OH^- + H_2O \qquad (22)$$

Model N Multiple electrochemical reaction

$$2Zn(OH)_4^= + 3e^- \rightleftharpoons Zn^0 + Zn(OH)_2^- + 6\ OH^- \qquad (23)$$

The mathematical treatments and other details of these models are given in appendix B. The mathematical treatments were aimed at finding sets of constants which would result in a zero plating current on the N planes at some cathodic voltage (implying positive values at higher voltages and negative values at lower voltages). The Butler-Volmer equations are given in table I and the important computer steps are listed in tables II, III, and IV. A wide variety of constants were tried (tables V and VI), but for most of the models, a zero value for the non-basal plating current required a negative value for either a rate constant (exchange current) or a concentration. Thus, models C, D, E, F, G, H, I, J, and N were found to be unacceptable. However, for certain positive values of constants for models B, K, L, and M, the non-basal plating current was zero at cathodic voltages, and the non-basal plating current was negative at lower cathodic voltages. In table VII, the sets and subsets for which this is true is indicated by a positive value for R_1. Thus, it is possible to have dissolution for certain planes in the cathodic region.

Once one knows that some models will work, it is interesting to examine the dependence of the various currents and other variables on voltage. The pertinent program steps are indicated in table VIII. We will look at one set of conditions for each workable model. A graphic survey of all the conditions (sets of constants) for which Np (plating current on the non-basal planes) = 0 is beyond the scope of this report.

Model B. - This model involves disproportionation, equation (11), along with the fundamental equations (model A). It was found to result in a feasible model only when disproportionation is very rapid on the N planes and nonexistent on the B plane; mathematically, $X_N \rightarrow 1$ ($X_N = 1$) and $B_6 = 0$.

6

In more practical terms this implies the N planes have a much higher catalytic activity than the B plane.

Figure 8 shows the dependence of various currents on overvoltage for this model for one particular set of constants (set 2, subset 0, $D_2 = 13.86$). In this and subsequent figures solid lines indicate currents in the plating direction and dashed lines indicate currents in the dissolving direction. In figure 8(a), the plating current B_p on the basal plane is well behaved: in the cathodic region plating occurs, and in the anodic region dissolution occurs. However, the plating current on the non-basal planes N_p exhibits the type of anomolous behavior that we have been seeking: at low cathodic voltages, dissolution occurs. At higher cathodic voltages and at anodic voltages, plating occurs on the N planes. Plating on the N planes at anodic voltages would be very difficult to observe.

It is easier to examine higher current - voltage behavior via the Tafel type plot in figure 8(b). In this figure, one sees that at sufficiently high cathodic voltages, the plating on the N planes exceeds that on the B plane due to an inflection of the slope of B_p in the 100 to 200 mV region. This satisfies the condition needed for dendrite formation. From figure 8(b), one also sees that at high anodic voltages the anomolous plating on the N planes in the anodic region finally changes to dissolution.

Figure 8(c) shows the overall Tafel plot that would be observed for the system; the log of the total current is plotted against the voltage. This illustrates that the anomolous behavior of individual planes would not show up in a Tafel experiment. Moreover, the Tafel slopes (fig. 8(c)) are in agreement with experimental values (ref. 8). At this time, we point out that the shape of the curves depend only on the ratio of rate constants and not on their absolute values. The absolute values affect the position of the curves on the current scale; that is they affect the value of the exchange current, i_0. Thus, any model can be adjusted so as to give an i_0 in agreement with the experimental data.

Finally, figure 8(d) shows the dependence on voltage of the individual non-basal plane current components: N_1, N_3, and N_5. The currents N_1 and N_3 exhibit conventional Tafel behavior at all voltages. It is N_5 that is responsible for all the anomolous behavior; N_5 is the cause of dissolution in the cathodic region and plating in the anodic region.

Models K, L, and M. - The chemistries of these three models are quite similar as seen from a comparison of equations (21) to (23). They differ only in the relative amounts of hydrogen and electron involvement in their auxiliary reaction, having in common all the fundamental plating reactions (model A). Model K is unique with respect to the other two in that its auxiliary reaction (eq. (21)) is not electrochemical.

Plating currents versus voltage curves are presented in figures 9, 10, and 11, respectively, for models K, L, and M. The sets of constants used are indicated in their respective table legends. The behavior shown for models K, L, and M is very similar to the type exhibited in figures 8(a) and (b) for model B. Current for the basal plane is again well behaved: cathodic in the cathodic region and anodic in the anodic region. The current for the non-basal plane is anodic in the low cathodic voltage region and cathodic in the low anodic voltage region. In higher cathodic voltage regions, the N current becomes cathodic. Model K at high anodic regions shows anodic behavior for the N planes which makes model K in complete qualitative agreement with model B as far as current voltage dependence is concerned. Perhaps models L and M

were not taken to a high enough anodic voltage for the N planes to exhibit anodic behavior in the anodic region. The very close similarity between models B and K could be attributable to the fact that both these models have nonelectrochemical auxiliary reactions, equations (11) and (20).

Although not shown, models K, L, and M exhibit conventional Tafel curves as does model B. And, for each of these models, the anomolous non-basal plane behavior is due to the N_5 current being in the opposite direction from N_3. Thus, at this point there is no grounds for a selection of a "best" model from among B, K, L, and M.

Effect of hydrogen. - There is one major difference between model B and models K, L, and M. Model B does not involve the presence of hydrogen (eq. (11)); the other three do (see eqs. (21) to (23)). Therefore, we examined the hydrogen activity for models K, L, and M as a function of voltage; table VIII outlines the procedure. Figure 12 shows the variety of dependencies that can be obtained. Hydrogen activity can increase with cathodic voltage and decrease with anodic voltage as in the case of model K. The activity can increase with both cathodic and anodic voltage; see conditions K'. Finally for models L and M, the hydrogen activity can increase with anodic voltage and decrease with cathodic voltage. If this is representative behavior of models L and M, for all combinations of constants, these models are not acceptable because hydrogen pressure (activity) is known to increase in the cathodic region of the alkaline zinc electrode. In contrast, model K is acceptable in that it predicts hydrogen formation at high cathodic voltages (dendritic region) as is generally observed. It has been reported (ref. 11) that the alkaline zinc electrode also evolves hydrogen at high anodic voltages. If this be the case model K is still acceptable because conditions K' predict the increased hydrogen pressure in both the anodic and cathodic regions.

Any of the models which involve hydrogen activity in their reactions will evolve hydrogen gas when the value of H corresponds to a pressure above atmospheric. This condition sets an upper limit to the value of H. For figure 13, the assumption was made of a fixed maximum for H for model K with conditions K' (for this condition hydrogen is produced in both the anodic and cathodic directions). The effect is that in the anodic region, Np switches from plating to dissolving at a lower voltage. Of more importance is the fact that a negligible effect occurs in the cathodic region; thus, ignoring the fact H may reach a maximum value does not affect any of our previous conclusions.

CONCLUDING REMARKS

From an examination of the appearance and crystal orientation of the various zinc deposits, we have postulated the following mechanism as an explanation for the variety of morphologies. The dendrite morphology produced at high current densities is a result of more rapid deposition on the non-basal crystallographic planes ($1\bar{1}00$, $10\bar{1}0$, and $01\bar{1}0$) than on the basal plane. The mossy morphology produced at low current densities is due to actual dissolution of zinc from the non-basal planes at low cathodic voltages. The boulder modification which forms at intermediate current densities results from comparable plating on both the basal and non-basal planes.

Fourteen electrochemical models were explored to account for such behavior. In all of these, the exchange currents, rate constants, etc., were allowed to have a variety of values and they were assumed to be different for

8

the basal and non-basal planes. The currents versus voltage were calculated via computer programs. A model consisting only of fundamental plating reactions can explain different rates on different planes but not dissolution from a plane in the cathodic voltage region. Each of the other models consists of the fundamental plating reactions plus an additional reaction. Only two of the models explored can account for the proposed mechanism. The one model involves very rapid disproportion of the $Zn(OH)_2^-$ intermediate to form zincate and zinc on the non-basal planes and no disproportionation on the basal plane. The second workable model involves a redox reaction between the zinc-zincate and hydrogen-water species. The second model can thus be used to explain the evolution of hydrogen at high cathodic voltages. It can also explain the hydrogen evolution at anodic voltages reported (ref. 11) for the alkaline zinc system. The two workable models give overall Tafel data in agreement with experimental work (ref. 9).

The general mechanism and models may be applicable to other metal systems with multiple morphologies. The metal involved must be at least divalent.

We again re-emphasize all the models assume steady state conditions. Model A involves only diffusion of the intermediate species, reaction (9), and the electrochemical zinc plating, reactions (1-2) and (3-4). Thus, equations (5) to (8) and equation (10) are involved. Equation (10) requires a little more discussion than given in the text proper.

$$D_1 = D_2 (X_N - X_B) \qquad (10)$$

For ease of manipulation, the D_1 is expressed in units of current per unit area to agree with the units in equations (5) to (8). D_2 has to be expressed in the same units. The D_2 comprises the diffusion coefficient, the length of border between basal and non-basal surface planes, and the surface areas of both sets of surface planes. In this paper we will not express D_2 in more detailed terms because of the complexities that would arise.

The important steps in the computer program are as follows:

Assign values to the constants (A1)

For v = -10 to -390   Step-20:   Rem V = millivolts;
    negative voltages are cathodic (A2)

$V = \exp (+0.01919v)$ (A3)

$B_7 = B_4/V^{BB} + B_2 V^{(2-BA)}$ (A4)

$B_8 = B_2/V^{BA} + B_4 V^{(2-BB)}$ (A5)

$N_7 = N_4/V^{NB} + N_2 V^{(2-NA)}$ (A6)

$N_8 = N_2/V^{NA} + N_4 V^{(2-NB)}$ (A7)

$D_1 = D_2 (N_8/N_7 - B_8/B_7)/(1 + D_2/N_7 + D_2/B_7)$ (A8)

$X_N = (N_8 - D_1)/N_7$ (A9)

$X_B = (B_8 + D_1)/B_7$ (A10)

Equations (5) to (8) (A11)

$R = N_3/B_3$ (A12)

Print values (A13)

To study model A, we have used four basic sets of constants that were in keeping with the Bockris electrochemical mechanism. Values of R were calculated as a function of overvoltage. Then, the effect of changing the value of one constant at a time was recorded. The plots of R versus v thus obtained are given in figures 4 to 7.

Some of the conclusions are given in the text proper. More details are given here. Some of the conclusions are obvious without even reference to these figures; some are not. When the N parameters (N_2, N_4, NA, NB) are

equal to the respective B parameters, R is unity independent of voltage (fig. 4(a)); and there is no dependence on D_2 (fig. 4(f)). If changing an N parameter has an effect, then changing the respective B parameter the same amount has about the same magnitude of effect but in the opposite direction. Compare figure 4(b) with 4(g); 4(d) with 4(i); 5(d) with 5(i); etc. Changing a constant for the fast step (one with a relatively high constant) has little or no effect on R, or on its dependence on v (see figs. 4(c), 4(e), 4(h), 4(j), 5(c), 5(e), 5(h), 5(j), etc.). Changing the ratio between the constant for the slow reaction on one plane with respect to that on the other plane changes the value of R; compare figure 4(b) with 4(a), 4(g) with 4(a), 5(b) with 5(a), 5(g) with 5(a), 6(b) with 6(a), etc. For these cases in figures 4 and 5, R becomes equal to N_2/B_2; for these cases in figures 6 and 7, R becomes equal to N_2/B_2 at the higher voltages. Appreciable changes in R with voltage arise from two conditions: (1) variations of an exponential constant of the rate determining step (NA and BA (figs. 4(d), 4(i), 5(d), and 5(i)); and (2) the condition of having $N_2 > N_4$ while $B_4 > B_2$ (figs. 6 and 7). Note that in figure 7 when $B_4 > N_2 > B_2 > N_4$, the values of R do cross the value of unity at some cathodic voltage. The curves in figure 7 indicate that at low voltages, plating on the basal planes can dominate and at high voltages, plating on the non-basal planes can dominate. If both an exponential constant varies from unity and $N_2 > N_4$ while $B_4 > B_2$, then the value of can reach a maximum at some voltage. (See figs. 6(i) and 7(i).)

In order for R to have a negative value, it must equal zero at some cathodic voltage. Thus,

$$N_3 = 0 \tag{A14}$$

Substituting this into equation (6)

$$X_N = V^2 \tag{A15}$$

Due to conservation of $Zn(OH)_2^-$ on each plane

$$D_1 = N_1 \tag{A16}$$

and

$$B_1 + D_1 = B_3 \tag{A17}$$

Substituting equations (5), (7), (8), and (10) into these equations

$$X_B = V^2 + (N_2 (V^4 - 1))/(D_2 V^{NA}) \tag{A18}$$

and

$$X_B = (B_8 + D_2 V^2)/(B_7 + D_2) \tag{A19}$$

The symbols B_7 and B_8 are defined in equations (A4) and (A5).

Combining these:

$$N_2/D_2 = ((B_8 + D_2 V^2)/(B_7 + D_2) - V^2) V^{NA}/(V^4 - 1) \tag{A20}$$

11

Because $N_2/D_2 > 0$ and $V^4 - 1 < 0$, then

$$(B_8 + D_2 V^2)/(B_7 + D_2) < V^2 \tag{A21}$$

Simplifying and substituting the values of B_7 and B_8 from equations (A4) and (A5)

$$V^2 > (B_4/V^{BB} + B_2 V^{(2-BA)})/(B_2/V^{BA} + B_4 V^{(2-BB)}) \tag{A22}$$

Additional simplification gives

$$V^4 > 1 \tag{A23}$$

But $V < 1$ in the cathodic region, so that $N_3 \neq 0$ in the cathodic region and thus for model A, there cannot be dissolution of metal on the non-basal plane in the cathodic region.

APPENDIX B - OTHER MODELS

Each model involves the reactions for model A; thus, for each model equations (1) to (10) are applicable. In addition, each model includes one of the reactions, equations (11) to (23). As a result, each model also has two additional mathematical (Butler-Volmer) relationships as given in table I: one for the basal planes and one for the non-basal planes. The N_5 and B_5 are the respective rates on the non-basal and basal planes. These are given in current per unit area for the sake of agreement with other equations used. The N_p is the total plating current on the N plane. The N_6 and B_6 are the corresponding rate constants. The NC and BC are equal twice the corresponding symmetry factors. The same set of symbols is used in each model to avoid complexities in symbol notation. The symbol H refers to the ratio of hydrogen activity at voltage v to its value at $v = 0$. The diffusion of hydrogen absorbed on the electrode surfaces was assumed to be much more rapid than that for the $Zn(OH)_2^-$ species so that the value of H was taken to be the same on both sets of planes. The expressions for N_5, B_6, and N_p were obtained by examining the respective chemical reaction, equations (11) to (23), as well as equations (1-2) and (3-4).

From the expressions in table I, equations (5) to (8) and (10), and the condition of steady state; computer programs were set up to calculate a ratio R_1 between two selected rate constants under the condition $N_p = 0$. The important steps in these programs are listed in table II for $D_2 = 0$. In general permitting $D_2 > 0$ would allow X_N to become closer to X_B in value and thus would nullify in part the effect of the auxiliary equations introduced into these models.

Only for models B, I, J, and N did the introduction of diffusion appear to be a possible way of improving the model, that is allowing it to exhibit $N_p = 0$ for some set of rate constants. We thus set up for models B, I, J, and N, computer programs for which D_2 was very large so that $X_N = X_B$: the essence of these programs are listed in table III.

For model B still another possibility exists because the auxiliary equation neither involves an electrode reaction nor the presence of the "foreign" species, hydrogen. Therefore, in model B, B_6 does not have to equal $-N_6$ (a necessity when H is produced at one surface used up at the other). We let $B_6 = 0$ and let N_6 have a very large value by setting $X_N = 1$, meaning $Zn(OH)_2^-$ was in equilibrium with Zn^0 and $Zn(OH)_4^{2-}$. The important computer steps are in table IV.

One must remember that $N_p = 0$ is not the only requirement for a feasible model. It is also necessary for $(\partial N_p / \partial v)_{R1}$ to be positive where $N_p = 0$. To determine this we made use of the following equation, all derivatives being evaluated at $N_p = 0$.

$$(\partial N_p / \partial v)_{R1} = - (\partial R_1 / \partial v) N_p / (\partial R_1 / \partial N_p)_v$$

Into each computer program, we inserted a subroutine involving the presence of a slight amount of plating on the non-basal plane, N_p, and thus determined whether $(\partial R_1 / \partial N_p)_v$ was positive or negative. The dependence of R_1 on v from our original program gives us the sign of $(\partial R_1 / \partial v) N_p$. In addition, we added another subroutine to ascertain if X_N, X_B, and H (hydrogen concentration in appropriate models) had positive values.

13

It is readily seen from the final equation in some of the programs (tables II, III, and IV) that the ratio R_1 between the rate constants determined is always negative regardless of the values of other constants. Thus, for these models, N_p can not be zero in the cathodic region. These models have been indicated by asterisks in tables II, and III; the models are models I and J with $D_1 = 0$ and model I and J with $X_N = X_B$. The programs of all the models were run using nine different sets of constants as shown in table V. By close examination of the equations one can determine that the actual value of the constants is not important in the calculation, only their relative values. For each set, each program was rerun with the change of one constant with respect to the original set. The changes are indicated in table VI. By this method we found that for models B, C, D, E, F, G, H, I, J, and N with $D_2 = 0$ and for models B, I, and N with $X_N = X_B$, it was not possible to have $N_p = 0$ in the cathodic region.

However, for some models and certain values of the constants, it was indeed found possible to have $N_p = 0$ in the cathodic region: these included models K, L, and M with $D_2 = 0$; and model B with $X_N = 1$ and $B_6 = 0$. The sets and subsets for which this is true ($N_p = 0$) are indicated in table VII by giving the value of R_1 for the condition $v = -10$ mV (10 mV cathodic). The programs showed that N_p is negative between 0 and -10 mV for the value of R_1 given in table VII. Some of the sets and subsets are redundant for a particular model because (as mentioned earlier) only the ratio of constants and not their actual values are important in finding the condition of $N_p = 0$.

14

REFERENCES

1. Oswin, Harry G.; and Blurton, K. F.: The Morphology of Zinc Electro-deposited from Alkaline Electrolyte. Zinc-Silver Oxide Batteries, Arthur Fleischer and John J. Lander, eds., John Wiley and Sons, Inc., 1971, pp. 63-85.

2. May, C. E.; Kautz, H. E.; and Sabo, B. B.: Relation of Morphology of Electrodeposited Zinc to Ion Concentration Profile. NASA TN D 8527, 1977.

3. Stachurski, Z. O. J.: Study to Investigate and Improve the Zinc Electrode for Spacecraft Electrochemical Cells. (QR-1, Yardney Electric Co.; NASA Contract NAS5-10231) NASA CR-89299, 1967.

4. Bockris, J. O'M.; Nagy, Z.; and Drazic, D.: On the Morphology of Zinc Electrodeposition from Alkaline Solution. J. Electrochem. Soc., vol. 120, no. 1, Jan. 1973, pp. 30-41.

5. Arouette, S.; Blurton, K. F.; and Oswin, H. G.: Controlled Current Deposition of Zinc from Alkaline Solution. J. Electrochem. Soc., vol. 116, no. 2, Feb. 1969, pp. 166-169.

6. Armstrong, R. D.; and Bell, M. F.: The Electrochemical Behavior of Zinc in Alkaline Solution. Electrochemistry, vol. 4, 1974, pp. 12-16.

7. Bozek, John M.: Structure and Function of an Inorganic-Organic Separator for Electrochemical Cells - Preliminary Study. NASA TM X-3080, 1974.

8. Diggle, J. W.; Despic, A. R.; and Bockris, J. O'M.: The Mechanism of the Dendritic Electrocrystallization of Zinc. J. Electrochem. Soc., vol. 116, no. 11, Nov. 1969, pp. 1503-1514.

9. Bockris, J. O'M.; Nagy, Z.; and Damjanovic, A.: On the Deposition and Dissolution of Zinc in Alkaline Solutions. J. Electrochem. Soc., vol. 119, no. 3, Mar. 1972, pp. 285-295.

10. Fielder, W. L.: The Alkaline Zinc Electrode As a Mixed Potential System. NASA TM 79235, 1979.

11. Ruetschi, P.: The Electrochemical Reactions in the Mercuric Oxide Zinc Cell. Power Sources 4, Research and Development in Non-Mechanical Electrical Power Sources, D. H. Collins, ed. Oriel Press, 1973, pp. 381-400.

TABLE I. – EQUATIONS FOR MODELS B TO N

Model	Expressions for		
	N_5	B_5	N_P
B	$N_6 (X_N^2 - 1)$	$B_6 (X_B^2 - 1)$	$N_3 + N_5$
C	$N_6 (X_N - H)$	$B_6 (X_B - H)$	N_3
D	$N_6 (1 - H X_N)$	$B_6 (1 - H X_B)$	$N_3 - N_5$
E	$N_6 (X_N - H^2 V^2)/V^{NC}$	$B_6 (X_B - H^2 V^2)/V^{BC}$	N_3
F	$N_6 (1 - H^2 X_N V^2)/V^{NC}$	$B_6 (1 - H^2 X_B V^2)/V^{BC}$	$N_3 - N_5$
G	$N_6 (X_N - H V^4)/V^{2NC}$	$B_6 (X_B - H V^4)/V^{2BC}$	$N_3 + N_5$
H	$N_6 (1 - H X_N V^4)/V^{2NC}$	$B_6 (1 - HX_B V^4)/V^{2BC}$	N_3
I	$N_6 X_N (X_N - V^2)/V^{NC}$	$B_6 X_B (X_B - V^2)/V^{BC}$	$N_3 + N_5$
J	$N_6 X_N (1 - X_N V^2)/V^{NC}$	$B_6 X_B (1 - X_B V^2)/V^{BC}$	N_3
K	$N_6 (H^3 - X_N)$	$B_6 (H^3 - X_B)$	$N_3 + N_5$
L	$N_6 (H^2 - X_N V^2)/V^{NC}$	$B_6 (H^2 - X_B V^2)/V^{BC}$	$N_3 + N_5$
M	$N_6 (H - X_N V^4)/V^{2NC}$	$B_6 (H - X_B V^4)/V^{2BC}$	$N_3 + N_5$
N	$N_6 (1 - X_N V^6)/V^{3NC}$	$B_6 (1 - X_B V^6)/V^{3BC}$	$N_3 + N_5$

TABLE II. - PROGRAMS WHEN $D_2 = 0$

[Those models marked with * can be seen to be invalid because R_1 = neg. number.]

Model B

Equations (A1) to (A7)

$$X_N = (N_2/V^{NA} - N_4/V^{2-NB})/(N_2 V^{2-NA} - N_4/V^{NB})$$

$$X_B = (-B_7 + sqr (B_7^2 + 8 B_6 (B_8 + 2 B_6)))/4 B_6$$

$$R_1 = (N_6/N_4) = (X_N - V^2)/(V^{NB}(1 - X_N^2))$$

Model C

Equations (A1) to (A7)

$$X_N = V^2$$

$$A = N_6 + B_6 + B_6^2/(B_7 + B_6)$$

$$B = N_6 X_N + (B_6 B_8/(B_7 + B_6))$$

$$H = B/A$$

$$R_1 = (N_6/N_2) = (1 - V^2 X_N)/(V^{NA} (X_N - H))$$

Model D

Equations (A1) to (A7)

$$X_N = 1/V^2$$

$$A = N_6 B_6 X_N$$

$$B = N_6 B_7 X_N + B_6(B_8 - N_6)$$

$$C = - B_7(N_6 + B_6)$$

$$H = (-B + sqr (B^2 - 4 AC))/2A$$

$$R_1 = (N_6/N_4) = (X_N - V^2)/V^{NB} (1 - X_N H)$$

TABLE II. – CONTINUED.

Model E

Equations (A1) to (A7)

$$X_N = V^2$$

$$A = V^2 - BC \ (N_6/V^{NC} + B_6/V^{BC} - B_6^2)/(B_7 \ V^{BC} + B_6)$$

$$B = N_6 \ X_N/V^{NC} + B_6 \ B_8/(B_7 \ V^{BC} + B_6)$$

$$H = sqr \ (B/A)$$

$$R_1 = (N_6/N_4) = (1 - X_N \ V^2) \ V^{NC-NA}/(X_N - H^2 \ V^2)$$

Model F

Equations (A1) to (A7)

$$X_N = V^{-2}$$

$$A = N_6 \ B_6 \ X_N \ V^4 - BC - NC$$

$$B = N_6 \ B_7 \ X_N \ V^2 - NC + B_6 \ (V^2 - BC) \ (B_6 - N_6/V^{NC})$$

$$C = - \ B_7 \ (B_6/V^{BC} + N_6/V^{NC})$$

$$H = sqr \ ((-B + sqr \ (B^2 - 4 \ A \ C)) \ / \ 2 \ A)$$

$$R_1 = (N_6/N_2) = (X_N - V^2) \ V^{NC-NB}/(1 - X_N H^2 V^2)$$

Model G

Equations (A1) to (A7)

$$X_N = V^{-2}$$

$$W = V^2$$

$$A = W^2(N_6/W^{NC} + B_6/W^{BC} - B)$$

$$B = N_6 X_N/W^{NC} + B_6 B_8/(B_7 W^{BC} + B_6)$$

$$H = B/A$$

$$R_1 = (N_6/N_4) = (V^2 - X_N) \ W^{NC}/(V^{NB}(X_N - HW^2))$$

Table II. - CONTINUED.

Model H

Equations (A1) to (A7)

$$X_N = V^2$$

$$W = V^2$$

$$A = X_N N_6 B_6 W^{(2 - BC - NC)}$$

$$B = N_6 B_7 X_N W^{(2 - NC)} + B_6 W^{(2 - BC)} (B_8 + N_6/W^{NC})$$

$$C = - B_7 (N_6/W^{NC} + B_6/W^{BC})$$

$$H = (-B + sqr (B^2 - 4AC))/2A$$

$$R_1 = (N_6/N_2) = (X_N V^2 - 1) W^{NC}/(V^{NA} (1 - X_N W^2)$$

Model I

Equations (A1) to (A7)

$$X_N = V^{-2}$$

$$*R_1 = (N_6/N_4) = (V^2 - X_N) V^{NC-NB}/(X_N - V^2) = - V^{NC-NB}$$

Model J

Equations (A1) to (A7)

$$X_N = V^2$$

$$*R_1 = (N_6/N_4) = (X_N V^2 - 1) V^{NC-NA}/(1 - X_N V^2) = - V^{NC-NA}$$

TABLE II. – CONCLUDED.

Models K, L, M, and N

Equations (A1) to (A7)

If K, then Q = 3:   If L, then Q = 2:   If M, then Q = 1:   If N, then Q = 0

$W = V^{3} - Q$

$X_N = (2N_4 \ V^{2 - NB} + N_2/V^{NA})/(2N_4/V^{NB} + N_2 \ V^{2 - NA})$

$B = N_6 \ X_N \ W^{2 - NC} + B_6 \ B_8 \ W^{2 - BC}/(B_7 + B_6 \ W^{2 - BC})$

$A = N_6/W^{NC} + B/W^{BC} - B_6^2 \ W^{2 - 2BC}/(B_7 + B_6 \ W^{2 - BC})$

If Q > 0, then $H = (B/A)^{1/Q}$

If 0 = 0, then H = 1

$R_1 = (N_6/N_4) = (X_N + V^2)/(V^{NB} (H^Q/W^{NC} - X_n \ W^{NC}))$

20

TABLE III. - PROGRAMS WHEN $X_N = X_B$

Model B

Equations (A1) to (A7)

$A = 2 B_6 + N_6$

$B = B_7 + N_2 V^2 - NA$

$C = - (B_8 + N_2/V^{NA} + A)$

$X_N = (-B + \text{sqr} (B^2 - 4AC))/2A$

$X_B = X_N$

$R_1 = (N_6/N_4) = (X_N - V^2)/(V^{NB} (1 - X_N{}^2))$

Model I

Equations (A1) to (A7)

$A = B_6/V^{BC}$

$B = B_4/V^{BB} - B_6 V^2 - BC + N_2 V^2 - NA + B_2 V^2 - BA$

$C = B_4 V^2 - BB - N_2/V^{NA} - B_2/V^{BA}$

$X_N = (-B + \text{sqr} (B^2 - 4AC))/2A$

$X_B = X_N$

$*R_1 = (N_6/N_4) = (V^2 - X_N) V^{NC-NB}/(X_N - V^2)) = - V^{NC-NB}/X_N$

Model J

Equations (A1) to (A7)

$X_N = V^2$

$X_B = X_N$

$*R_1 = (N_6/N_2) = -(V^{NC}/N_2)(B_6/V^{BC} + B_2/(X_N V^{BA}) + N_2/(X_N V^{NA}))$

21

TABLE III. - CONCLUDED.

Model N

Equations (A1) to (A7)

$$W = V^3$$

$$A = B_4/V^{BB} + B_6W^2 - BC + B_2V^2 - BA + 2N_6W^2 - NC + N_2V^2 - NA$$

$$B = B_4/V^2 - BB + B_6/W^{BC} + B_2/V^{BA} + 2N_6/V^{NC} + N_2/V^{NA}$$

$$X_N = B/A$$

$$X_B = X_N$$

$$*R_1 = (N_6/N_4) = (V^2 - X_N) W^{NC}/(V^{NB} (1 - X_N W^2))$$

TABLE IV. – PROGRAM WHEN $B_6 = 0$ AND $X_N = 1$

Model B

Equations (A1) to (A7)

$X_N = 1$

$N_1 = N_2 (1 - V^2)/V^{NA}$

$N_3 = N_4 (1 - V^2)/V^{NB}$

$D_1 = N_1 + N_3$

$X_B = (B_8 + D_1)/B_7$

$R_1 = D_2 = D_1/(1 - X_B)$

TABLE V. - SETS OF CONSTANTS USED

Set	B_2	B_4	N_2	N_4	Value of all other constants
1	1	100	1	100	1
2	1	100	.1	10	1
3	1	100	10	.1	1
4	1	100	100	1	1
5	100	1	1	100	1
6	100	1	.1	10	1
7	1	100	1000	10	1
8	100	1	100	1	1
9	100	1	10	1000	1

TABLE VI. - VARIATIONS OF CONSTANTS

Subset	Value
0	As indicated in table I
1	N_2 = 10 times value of N_2 in set
2	N_4 = 10 times value of N_4 in set
3	NA = 0.8
4	NB = 0.8
5	B_2 = 10 times value of B_2 in set
6	B_4 = 10 times value of B_4 in set
7	BA = 0.8
8	BB = 0.8
9	NC = 0.8
10	B_6 = 10
11	BC = 0.8

TABLE VII. - VALUES OF R_1 FOR WHICH N_p = 0 AT v = 10 mV

[- indicates negative values]

Set \ Subset	0	1	2	3	4	5	6	7	8	9	10	11
Model B (B_6 = 0 and X_N = 1)												
1	-	-	-	-	6719	-	136.4	-	-	-	-	-
2	13.86	15.25	-	13.85	13.29	16.36	12.38	13.85	13.93	13.86	13.86	13.86
3	-	-	-	6719	-	-	136.3	-	-	-	-	-
4	13.86	-	15.28	13.29	13.85	16.36	12.38	13.85	13.93	13.86	13.86	13.86
5 to 9	-	-	-	-	-	-	-	-	-	-	-	-
Model K												
1,2	-	3.062	-	-	-	-	3.032	-	-	-	-	-
3,4,7	2.450	2.450	2.455	2.450	2.358	2.603	2.426	2.449	2.451	2.451	1.352	2.450
5,6,9	-	-	-	-	-	-	-	-	-	-	-	-
8	-	210.6	-	-	-	-	23.79	-	-	-	-	-
Model L												
1,2	-	3.707	-	-	-	-	3.673	-	-	.07653	-	-
3,4,7	2.966	2.966	2.972	2.966	2.855	3.152	2.939	2.966	2.967	2.328	1.636	3.024
5,6,8,9	-	-	-	-	-	-	-	-	-	-	-	-
Model M												
1,2	-	4.489	-	-	-	-	4.450	-	-	.04574	-	-
3,4,7	3.592	3.591	3.598	3.592	3.456	3.817	3.560	3.591	3.593	2.319	1.980	3.735
5,6,9	-	-	-	-	-	-	-	-	-	-	-	-
8	-	308.6	-	-	-	-	34.86	-	-	6.268	-	-

TABLE VIII. - STEPS FOR CALCULATING CURRENTS

VALUES AS A FUNCTION OF VOLTAGE

Model B ($X_N = 1$; $B_6 = 0$)

Assign values to constants
Assign value to D_2 which makes $N_p = 0$ at $v = -10$ mv
For $v = -30$ to $+30$ step 2 [or for -300 to $+300$ step 20]
Equations (A3) to (A11)
Appropriate expressions for B_5 and N_6 from table I
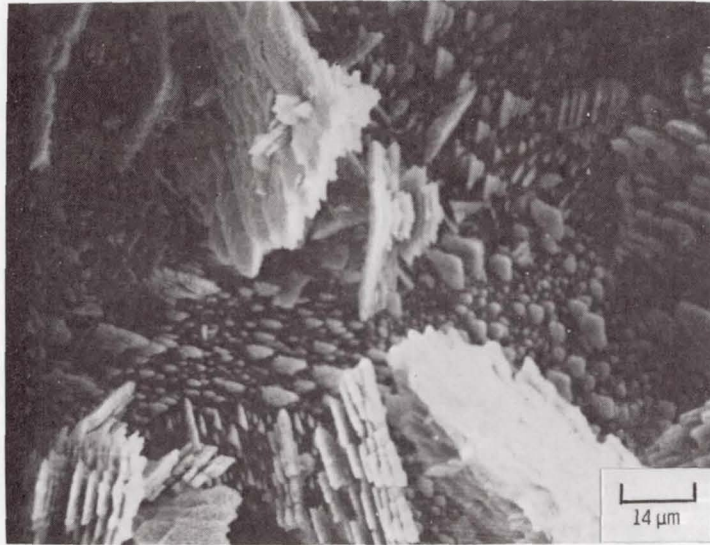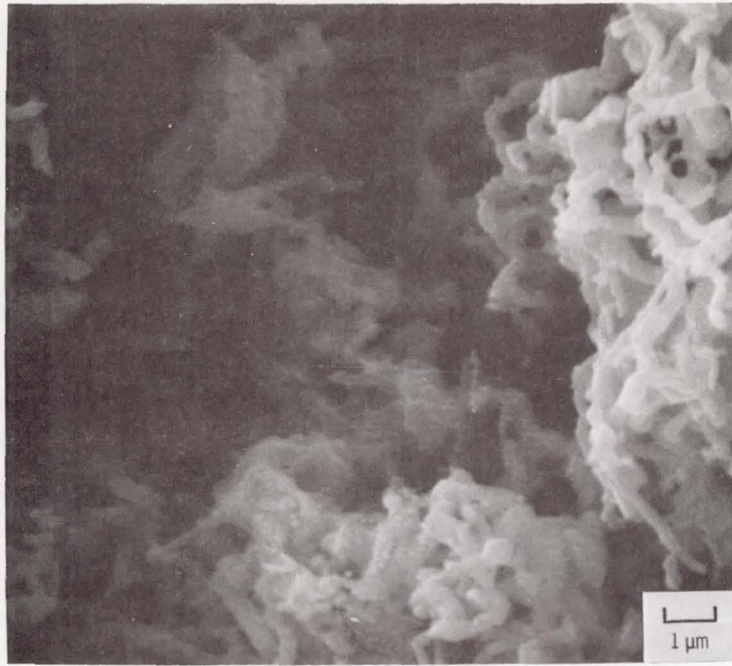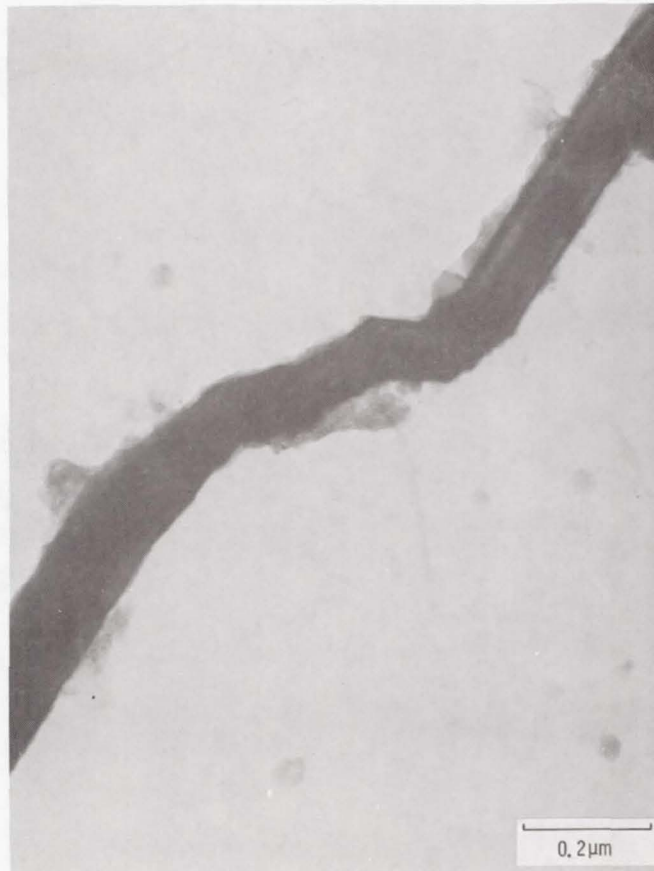Print Results

Model K, L, and M ($D_2 = 0$)

Assign values to constants
Assign value to R_1 which makes $N_p = 0$ at $v = -10$ mv
Let $N_4 = R_1 N_6$
Let $N_2 = N_4$ times original value of N_2/N_4
For $v = -30$ to $+30$ step 2 [or for -300 to $+300$ step 20]
Equations (A3) to (A11)
Appropriate expressions for B_5 and N_6 from table I
Print Results

Figure 1. - SEM view of dendritic zinc deposit.

(a) SEM VIEW OF MOSSY ZINC DEPOSIT.

(b) TEM VIEW OF MOSSY ZINC SINGLE CRYSTAL.

Figure 2.
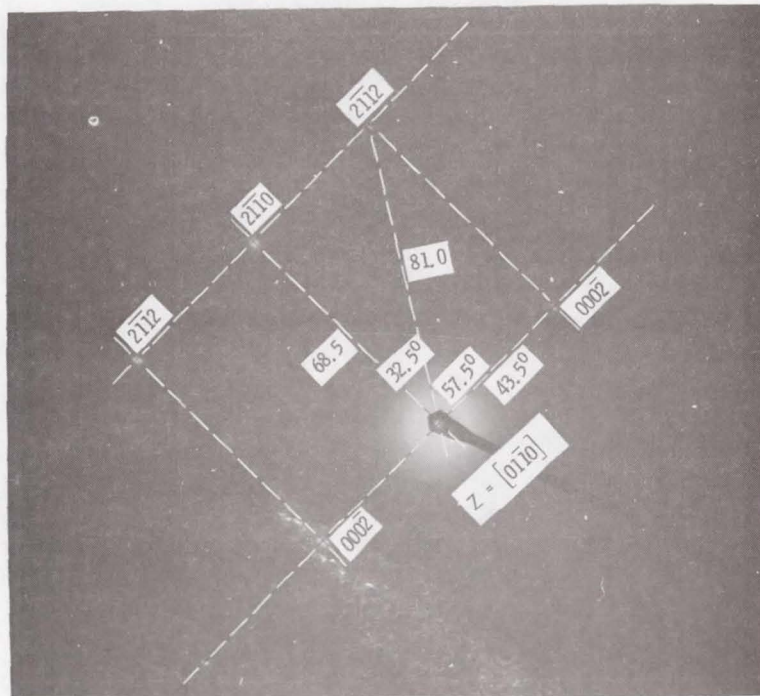
(c) ELECTRON DIFFRACTION PATTERN OF ZINC MOSS CRYSTAL OF FIGURE 2(b).
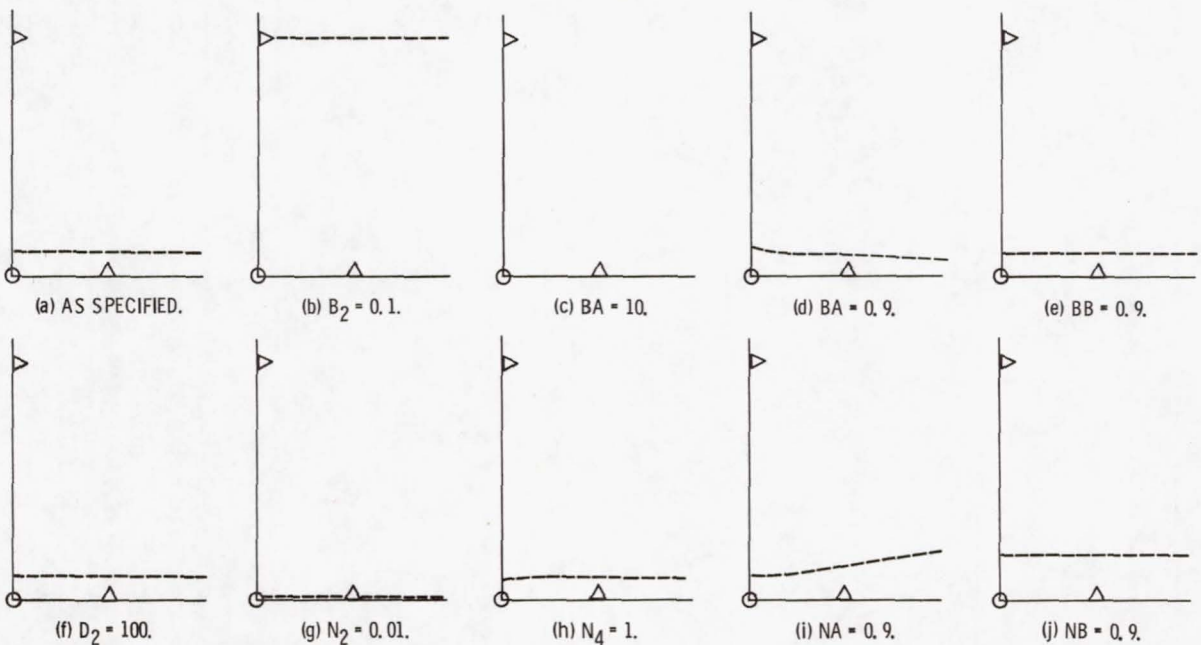
Figure 2. - Concluded.
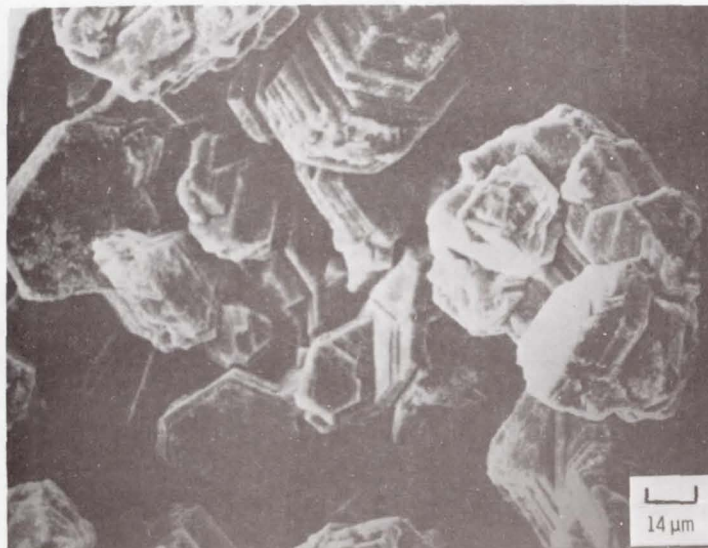
Figure 3. - SEM view of zinc boulder deposit.
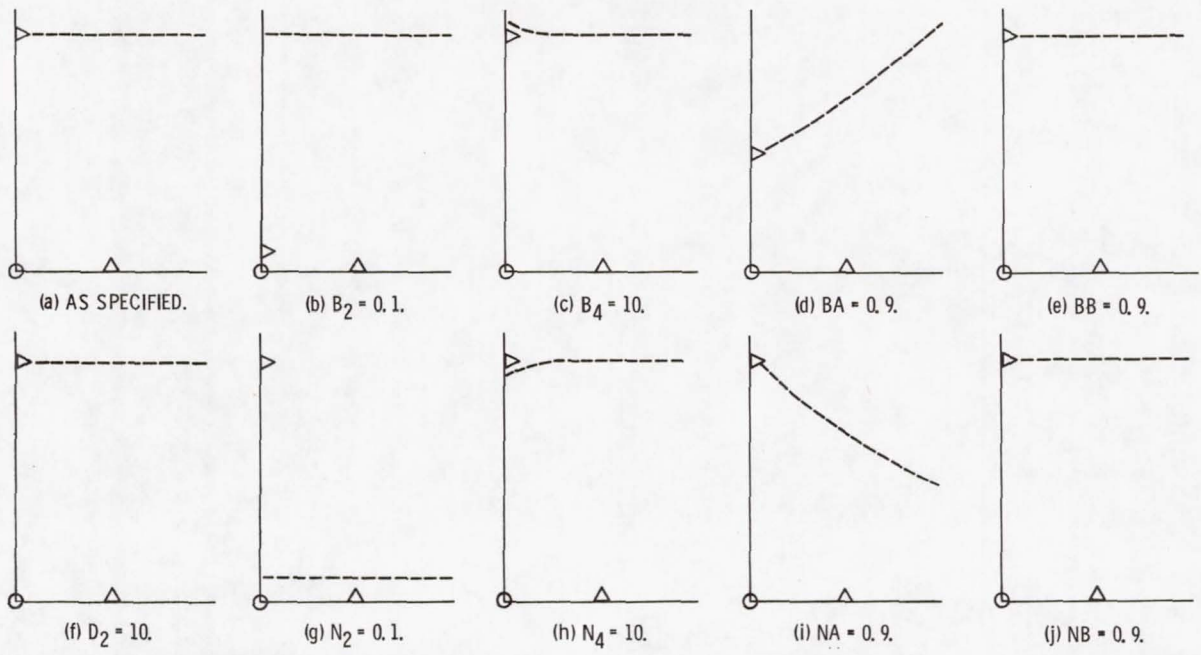
Figure 4. – Ratio (R) of plating on nonbasal plane to basal plane as a function of voltage: Model A ▷ locates R = 1; △ locates -200 mV; unless otherwise specified: $B_2 = 1$; $B_4 = 100$; $BA = 1$; $BB = 1$; $N_2 = 1$; $N_4 = 100$; $NA = 1$; $NB = 1$; and $D_2 = 0$).
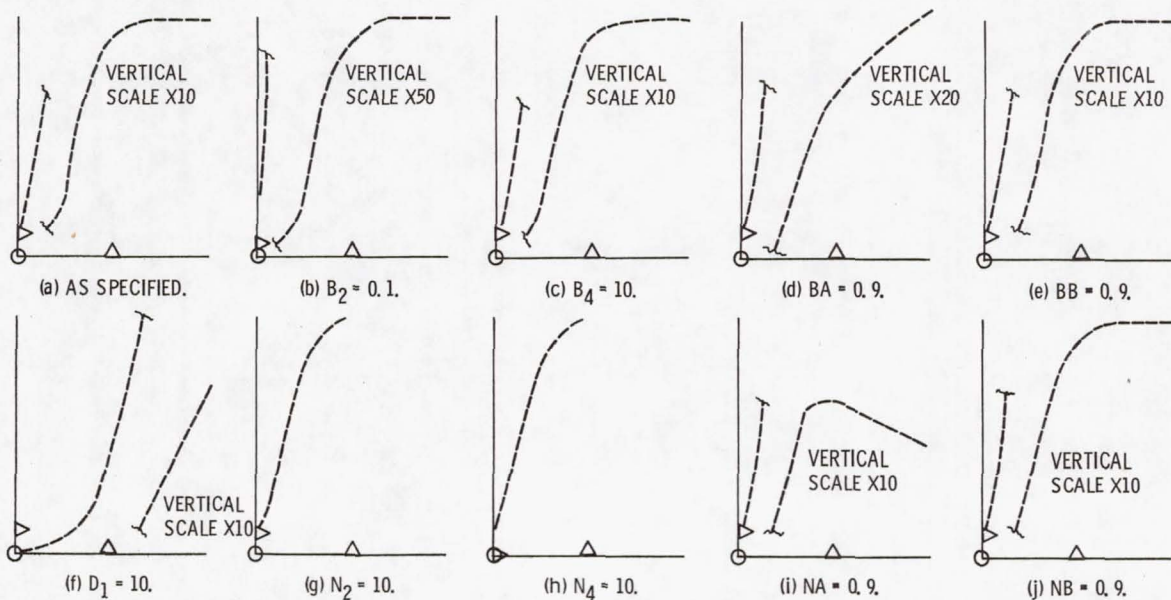
(a) AS SPECIFIED.

(b) $B_2 = 0.1$.

(c) $B_4 = 10$.

(d) $BA = 0.9$.

(e) $BB = 0.9$.

(f) $D_2 = 10$.

(g) $N_2 = 0.1$.

(h) $N_4 = 10$.

(i) $NA = 0.9$.

(j) $NB = 0.9$.

Figure 5. – Ratio (R) of plating on nonbasal plane to basal plane as a function of voltage: Model A ▷ locates R = 1; △ locates -200 mV; unless otherwise specified: $B_2 = 1$; $B_4 = 100$; $BA = 1$; $BB = 1$; $N_2 = 0.1$; $N_4 = 10$; $NA = 1$; $NB = 1$; and $D_2 = 0$).

(a) AS SPECIFIED.

(b) $B_2 = 0.1$.

(c) $BA = 10$.

(d) $BA = 0.9$.

(e) $BB = 0.9$.

(f) $D_2 = 100$.

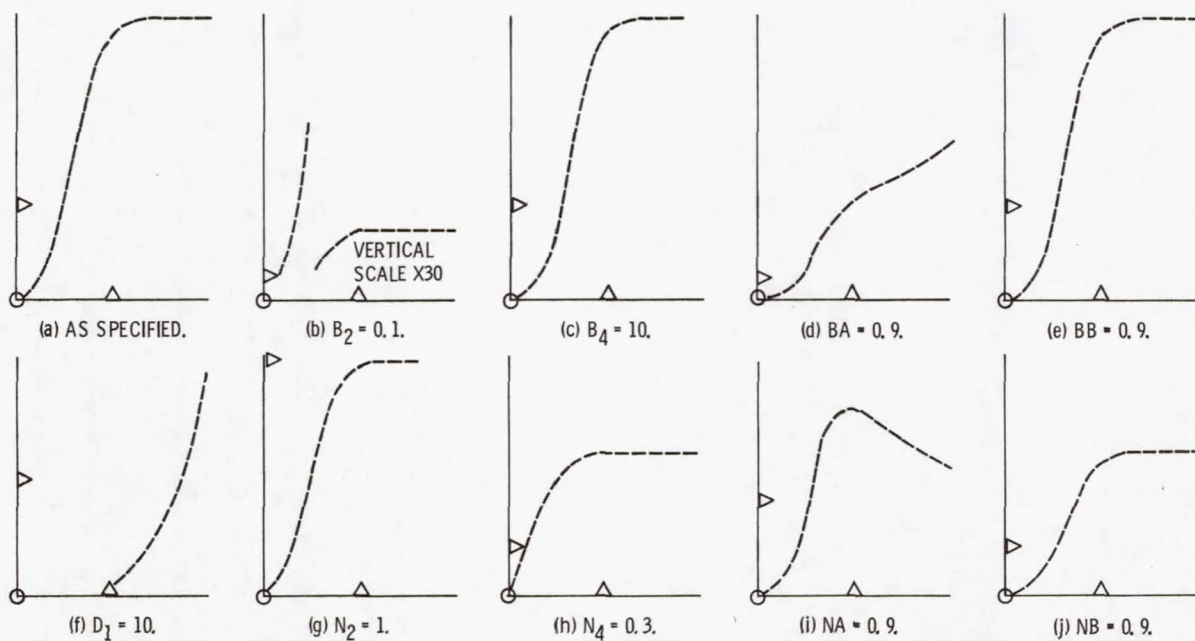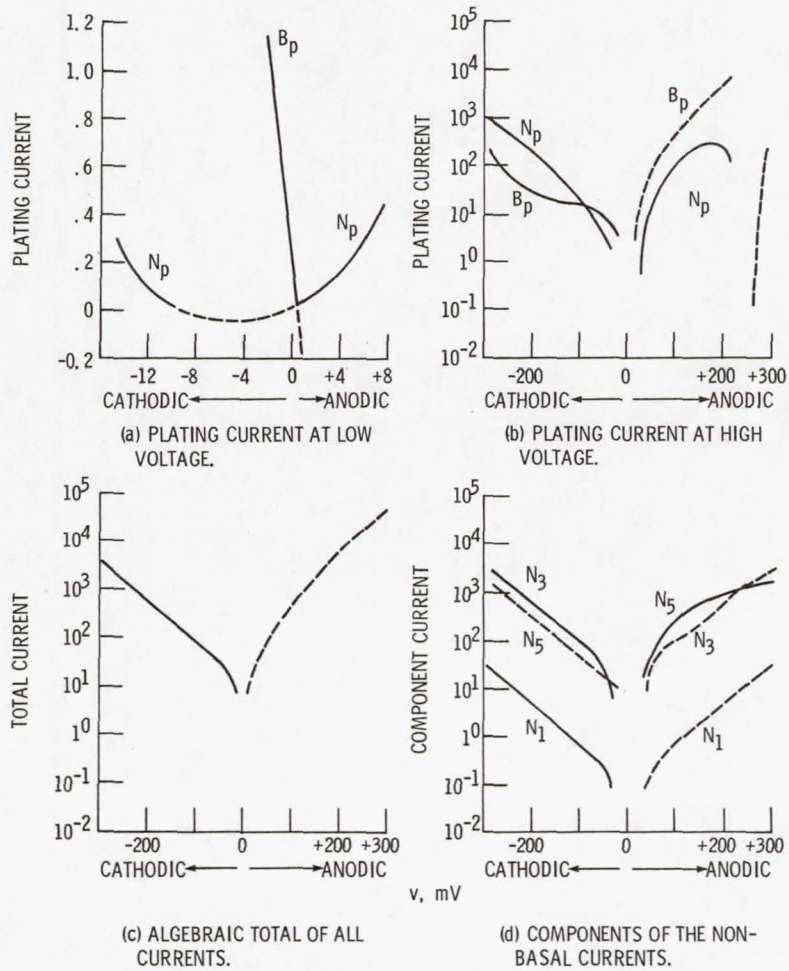(g) $N_2 = 0.01$.

(h) $N_4 = 1$.

(i) $NA = 0.9$.

(j) $NB = 0.9$.

Figure 6. – Ratio (R) of plating on nonbasal plane to basal plane as a function of voltage; Model A ($\triangleright$ locates R = 1; $\triangle$ locates -200 mV; unless otherwise specified: $B_2 = 1$; $B_4 = 100$; BA = 1; BB = 1; $N_2 = 100$; $N_4 = 1$; NA = 1; NB = 1; and $D_2 = 0$).

Figure 7. – Ratio (R) of plating on nonbasal plane to basal plane as function of voltage: Model A ($\triangleright$ locates R = 1; $\triangle$ locates -200 mV; unless otherwise specified: $B_2 = 1$; $B_4 = 100$; BA = 1; BB = 1; $N_2 = 3.0$; $N_4 = 0.03$; NA = 1; NB = 1; $D_2 = 0$).

(a) PLATING CURRENT AT LOW VOLTAGE.

(b) PLATING CURRENT AT HIGH VOLTAGE.

(c) ALGEBRAIC TOTAL OF ALL CURRENTS.

(d) COMPONENTS OF THE NON-BASAL CURRENTS.

Figure 8. - Current vs. voltage curves for Model B. (Solid line = plating direction; dashed = dissolving direction; $B_2 = 1$, $B_4 = 100$, $N_2 = 0.1$, $N_4 = 10$, $B_6 = 0$, $N_6 = \infty$, $BA = BB = NA = NB = 1$, $X_N = 1$, $D_2 = 13.86$; rate constant units are arbitrary, same as currents.)
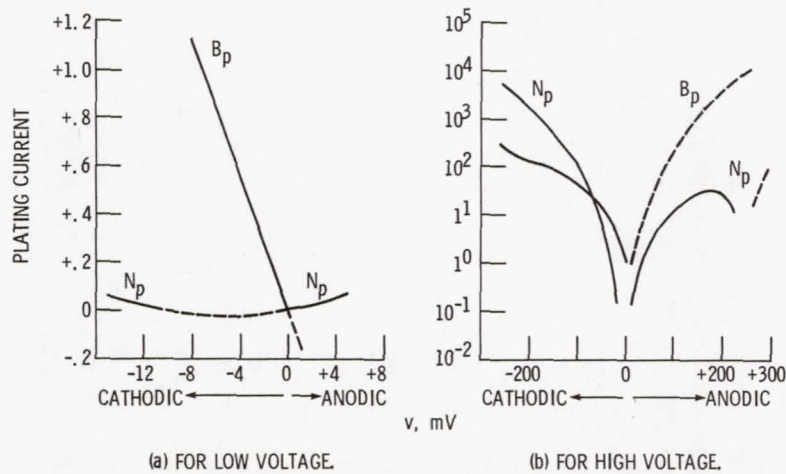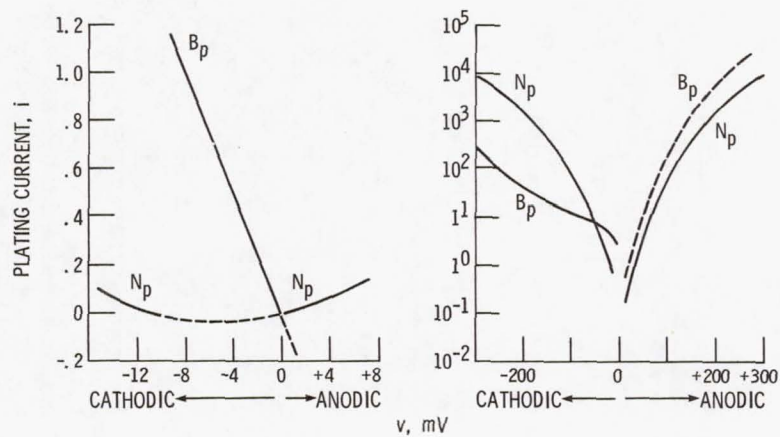

(a) FOR LOW VOLTAGE.

(b) FOR HIGH VOLTAGE.

Figure 9. - Plating current vs. voltage curves for Model K. (Solid line indicates current in the plating direction; dashed line indicates current in the dissolving direction; $B_2 = 1$, $B_4 = 100$, $B_6 = N_6 = 1$, $BA = BB = NA = NB = 1$, $D_2 = 0$, $R_1 = 2.450$, $N_4 = N_6/R_1$, and $N_2 = 100 N_4$; rate constant units are arbitrary, but the same as for currents.)
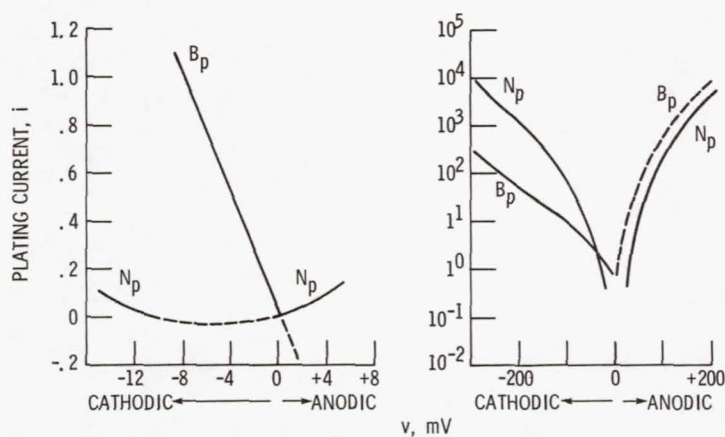
(a) FOR LOW VOLTAGE.

(b) FOR HIGH VOLTAGE.

Figure 10. - Plating current vs. curves for Model L. (Solid line indicates current in the plating direction; dashed line indicates current in the dissolving direction; $B_2 = 1$, $B_4 = 100$, $B_6 = N_6 = 1$, $BA = BB = NA = NB = 1$, $D_2 = 0$, $R_1 = 2.966$, $N_4 = N_6/R_1$, and $N_2 = 100 N_4$; rate constant units are arbitrary, but the same as for the currents.)

(a) FOR LOW VOLTAGE.

(b) FOR HIGH VOLTAGE.

Figure 11. - Plating current vs. voltage curves for Model M. (Solid line indicates current plating in the plating direction; dashed line indicates current in the dissolving direction; $B_2 = 1$, $B_4 = 100$, $B_6 = N_6 = 1$, $BA = BB = NA = NB = 1$, $D_2 = 0$, $R_1 = 3.592$, $N_4 = N_6/R_1$, and $N_2 = 100 N_4$; rate constant units are arbitrary, but the same as for the currents.)
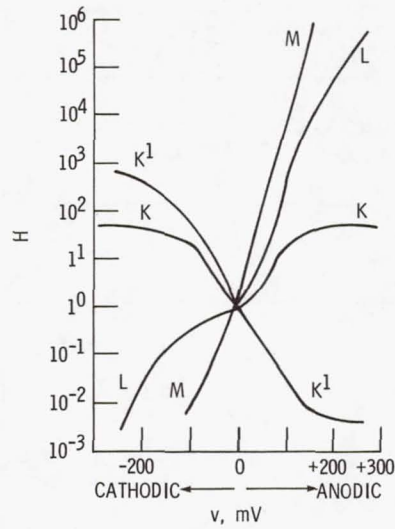
Figure 12. - Hydrogen activity relative to its equilibrium value. The constants for curves K, L, and M are given respectively in figures 9, 10, and 11. K^1 constants are those of Model K, set 1, subset 6.
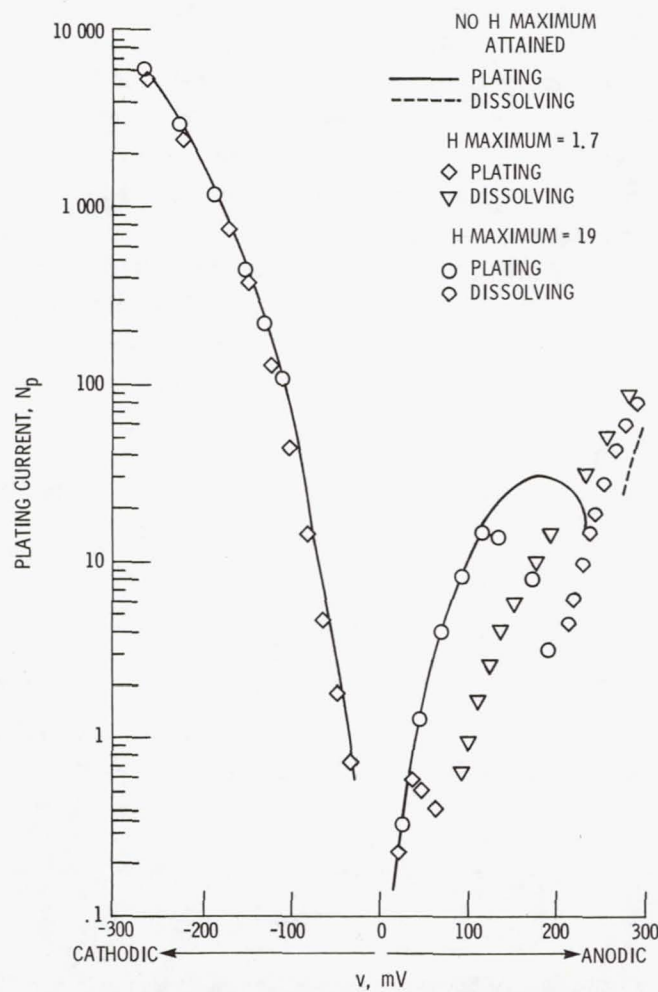

Figure 13. - Effect of a maximum hydrogen activity on N_p for Model K (set 1, subset 6).

1. Report No. NASA TM-82768	2. Government Accession No.	3. Recipient's Catalog No.
4. Title and Subtitle MECHANISM AND MODELS FOR ZINC METAL MORPHOLOGY IN ALKALINE MEDIA		5. Report Date December 1981
		6. Performing Organization Code 506-53-12
7. Author(s) Charles E. May and Harold E. Kautz		8. Performing Organization Report No. E-1090
		10. Work Unit No.
9. Performing Organization Name and Address National Aeronautics and Space Administration Lewis Research Center Cleveland, Ohio 44135		11. Contract or Grant No.
		13. Type of Report and Period Covered Technical Memorandum
12. Sponsoring Agency Name and Address National Aeronautics and Space Administration Washington, D.C. 20546		14. Sponsoring Agency Code

15. Supplementary Notes

16. Abstract

Based on experimental observations, a mechanism is presented to explain the existence of the different morphologies of electrodeposited zinc in alkaline solution. The high current density dendrites appear to be due to more rapid growth on the non-basal crystallographic planes than on the basal plane. The low current density moss apparently results from dissolution from the non-basal planes at low cathodic voltages. Electrochemical models were sought which would produce such a phenomenon. The fundamental plating mechanism alone can account only for different rates on different planes, not for zinc dissolution from a plane in the cathodic region. Fourteen models were explored; two models were found to be in accord with the proposed mechanism. One involves rapid disproportionation of the zinc +1 species on the non-basal planes. The other involves a redox reaction (corrosion) between the zinc-zincate and hydrogen-water systems.

17. Key Words (Suggested by Author(s)) Batteries Zinc electrode electrochemistry Plating morphology	18. Distribution Statement Unclassified - unlimited STAR Category 44		
19. Security Classif. (of this report) Unclassified	20. Security Classif. (of this page) Unclassified	21. No. of Pages	22. Price*

* For sale by the National Technical Information Service, Springfield, Virginia 22161

National Aeronautics and
Space Administration

Washington, D.C.
20546

SPECIAL FOURTH CLASS MAIL
BOOK

Postage and Fees Paid
National Aeronautics and
Space Administration
NASA-451

NASA

POSTMASTER: If Undeliverable (Section 158
Postal Manual) Do Not Return